Available online at www.sciencedirect.com
ScienceDirect
Journal of Computational Physics 218 (2006) 860–877
JOURNAL OF COMPUTATIONAL PHYSICS
www.elsevier.com/locate/jcp

A discontinuous Galerkin method for the Cahn–Hilliard equation

Garth N. Wells [a,*], Ellen Kuhl [b], Krishna Garikipati [c]

[a] Faculty of Civil Engineering and Geosciences, Delft University of Technology, Stevinweg 1, 2628 CN Delft, Netherlands
[b] Chair of Applied Mechanics, Technische Universität Kaiserslautern, Postfach 3049, D-67653 Kaiserslautern, Germany
[c] Department of Mechanical Engineering and Program in Applied Physics, University of Michigan, Ann Arbor, Michigan 48109, USA

Received 22 September 2005; received in revised form 14 March 2006; accepted 15 March 2006
Available online 5 May 2006

Abstract

A discontinuous Galerkin finite element method has been developed to treat the high-order spatial derivatives appearing in the Cahn–Hilliard equation. The Cahn–Hilliard equation is a fourth-order nonlinear parabolic partial differential equation, originally proposed to model phase segregation of binary alloys. The developed discontinuous Galerkin approach avoids the need for mixed finite element methods, coupled equations or interpolation functions with a high degree of continuity that have been employed in the literature to treat the fourth-order spatial derivatives. The variational formulation of the discontinuous Galerkin method, its implementation and numerical examples are presented. In this communication, it is also shown under what conditions the method is stable, and an error estimate in an energy-type norm is presented. The method is evaluated by comparison with a standard finite element treatment in which the Cahn–Hilliard equation is decomposed into two coupled partial differential equations.

Keywords: Phase segregation; Spinodal decomposition; Diffuse interface theory; Finite element methods; Parabolic partial differential equations

1. Introduction

Originally derived for phase segregation of a binary alloy system, the Cahn–Hilliard equation [1] has been applied to a wide range of problems, including multiphase fluid flow [2,3], image processing [4] and planet formation [5]. Additionally, viewing a single-species solid as a binary atom-vacancy mixture, the formation of void lattices has been modelled as a process of vacancy segregation by the Cahn–Hilliard treatment coupled with elastic effects [6]. These are just a few representative examples of a vast body of literature on applications of the Cahn–Hilliard equation.

* Corresponding author. Tel.: +31 15 278 7922; fax: +31 15 278 6383.
E-mail address: g.n.wells@tudelft.nl (G.N. Wells).

0021-9991/$ - see front matter
doi:10.1016/j.jcp.2006.03.010

Numerical solution techniques for the Cahn–Hilliard equation have spanned finite difference methods, spectral formulations and finite element methods. In this paper, the focus is on finite element methods. Previous finite element formulations have focused on the case wherein the Cahn–Hilliard equation has been rewritten as a coupled system of two partial differential equations (see for example [7–11]). In Bansch et al. [12] surface diffusion is treated by decomposing the governing fourth-order equation into a system of four partial differential equations, of which two are second-order and the remaining are zeroth-order. Also of interest is Ubachs et al. [13], where the concentration gradient-dependent free-energy, which forms the basis of the Cahn–Hilliard model, is replaced with a nonlocal free-energy. The resulting problem consists of two coupled second-order partial equations, which are solved using the standard Galerkin finite element method. In contrast stand the works of Elliott and Zheng [14], in which a conforming C^1 finite element method was examined, and Elliott and French [15], who used a non-conforming finite element method, inspired by mixed methods for thin plate problems.

The decomposition of the Cahn–Hilliard equation into two second-order partial differential equations follows the classical approach for the treatment of high-order differential equations using mixed finite element methods (see [16] for an overview). It avoids difficulties with the representation of high-order derivatives across element boundaries. Specifically, C^0 interpolations can be applied. Here, an alternate approach is followed in which a discontinuous Galerkin formulation is proposed which avoids the need for C^1 basis functions and allows the use of standard C^0 finite element shape functions. The standard weak form of the Cahn–Hilliard equation contains spatial derivatives up to and including order two in both the trial and weighting functions. A naive implementation with standard C^0 interpolations leads to terms involving the multiplication of Dirac-Delta functions on inter-element edges. Such terms are meaningless, even in a distributional sense. Instead of grappling with these difficulties, we aim to lay down a weak form that allows, at the outset, for fields in which the first derivative is discontinuous across element boundaries, but is consistent with the governing Cahn–Hilliard equation. This is achieved by the definition of suitable flux terms involving the normal derivatives across element boundaries in the weak form.

The proposed approach for the Cahn–Hilliard equation is inspired by works on discontinuous Galerkin methods for second-order elliptic equations, known as the 'interior penalty method', early examples of which can be found in [17–20]. These methods were developed largely separate from discontinuous Galerkin methods for first-order hyperbolic equations and discontinuous Galerkin methods in time. While discontinuous Galerkin methods for advection problems became well-accepted and proved to be effective, work on discontinuous Galerkin methods for elliptic problems was largely dormant. A wish to treat advective and diffusive terms using the same basis functions lead to a recent resurgence in interest for discontinuous Galerkin methods for elliptic problems. Overviews of works on discontinuous Galerkin methods for elliptic problems and extensive literature surveys can be found in Arnold et al. [21] and Engel et al. [22]. The approach followed here is a natural extension of recent work on discontinuous Galerkin formulations for fourth-order elliptic problems in structural mechanics (thin beam and plate theories) and strain gradient elasticity [22], and strain gradient damage [23,24].

The organisation of the paper is as follows: The Cahn–Hilliard equation is introduced in Section 2 and discontinuous and mixed Galerkin formulations are presented in Section 3. The numerical implementation of the discontinuous Galerkin formulation is discussed in Section 4, along with a conventional mixed finite element formulation. Numerical examples are solved in Section 5 to compare the discontinuous Galerkin and conventional formulations. Conclusions and a discussion in Section 6 complete the paper.

2. The strong form of the Cahn–Hilliard equation

Consider a binary mixture and let the concentration of one of its constituents, say A, be denoted by c satisfying $0 < c < 1$. The composition of the other constituent, B, is $1 - c$. Pure phases are obtained for $c = 0$ and $c = 1$. Let the mixture occupy an open, simply connected region in space, $\Omega \subset \mathbb{R}^d$, where $d = 1$, 2 or 3. The boundary of Ω is supposed to be sufficiently smooth, and is denoted by $\Gamma = \partial\Omega$, with outward unit normal $\boldsymbol{n}$. Further, let $\Gamma = \overline{\Gamma_g \cup \Gamma_s} = \overline{\Gamma_q \cup \Gamma_r}$, where $\Gamma_g \cap \Gamma_s = \Gamma_q \cap \Gamma_r = \emptyset$. Mass transport in the mixture is governed by a parabolic partial differential supplemented by initial and boundary conditions. In strong form we have the following problem: find $c : \overline{\Omega} \times [0, T] \to \mathbb{R}$ such that

$$c_{,t} = \nabla \cdot (M\nabla(\mu_c - \lambda\nabla^2 c)) \quad \text{in } \Omega \times (0,T), \tag{1}$$

$$c = g \quad \text{on } \Gamma_g \times (0,T), \tag{2}$$

$$M\lambda\nabla c \cdot \boldsymbol{n} = q \quad \text{on } \Gamma_q \times (0,T), \tag{3}$$

$$M\lambda\nabla^2 c = r \quad \text{on } \Gamma_r \times (0,T), \tag{4}$$

$$M\nabla(\mu_c - \lambda\nabla^2 c) \cdot \boldsymbol{n} = s \quad \text{on } \Gamma_s \times (0,T), \tag{5}$$

$$c(\boldsymbol{x},0) = c_0(\boldsymbol{x}) \quad \text{in } \Omega. \tag{6}$$

Here, $M > 0$ is known as the mobility, μ_c is the chemical potential of a regular solution in the absence of phase interfaces (a uniform solution, which may be interpreted as a solution in which c is spatially constant) and is a function of c, and $\lambda > 0$ is a constant that determines the magnitude of interface free-energy in the presence of a given concentration gradient. Eqs. (2) and (3) are boundary conditions on the concentration and its normal derivative, respectively. The less familiar Eq. (4) is effectively a boundary condition on a component of the total potential, as will be clarified below, while Eq. (5) is the flux boundary condition.

While the boundary conditions have been presented in a general form, the condition $\nabla c \cdot \boldsymbol{n} = 0$ on Γ was assumed in the original derivation of the Cahn–Hilliard equation. To be consistent with the thermodynamic derivation of the equation, $\Gamma_q = \Gamma$ and $q = 0$ is required.

In the following sections, two cases for the scalar M are considered. In the first, $M = D$ where D is the diffusivity and is constant. In the second case, the mobility is dependent on the concentration. The commonly adopted relationship

$$M = Dc(1-c), \tag{7}$$

in which D is again constant, is used. This relationship restricts diffusion processes primarily to the interfacial zones, and is commonly known as 'degenerate mobility'.

Remarks

(1) Eqs. (2)–(5) are the appropriate boundary conditions only for $\lambda > 0$. If $\lambda = 0$, only (2) and (5) are of relevance.
(2) The problem as posed is nonlinear due to the composition-dependent mobility M, and the nonlinearity in chemical potential μ_c.

The Cahn–Hilliard equation is derived by considering additive contributions to the total free-energy Ψ from a chemical term Ψ^{c} and a surface free-energy term Ψ^{s}. A potential μ_c is given by the functional derivative of the chemical free-energy with respect to the concentration, $D_c\Psi^{\mathrm{c}}$, and it is assumed that diffusion is driven by gradients in the total potential. Here, the chemical free-energy of a solution is considered to be given by [1]

$$\Psi^{\mathrm{c}} = NkT(c\ln c + (1-c)\ln(1-c)) + N\omega c(1-c), \tag{8}$$

where N is the number of molecules per unit volume, k is Boltzmann's constant, T is the absolute temperature and ω is a parameter related to the mixing enthalpy that determines the shape of Ψ^{c}. For $\omega > 2kT$, the chemical free energy is non-convex, with two wells which drives phase segregation into the two binodal points. For $\omega \leqslant 2kT$ it has a single well and admits a single phase only. A typical function for the chemical free-energy for the non-convex case is illustrated in Fig. 1.

According to the original model of Cahn and Hilliard [1], the surface free energy is given by

$$\Psi^{\mathrm{s}} = \frac{1}{2}\lambda\nabla c \cdot \nabla c. \tag{9}$$

It is this term which leads to the fourth-order derivatives in the Cahn–Hilliard equation. Details of the derivation of the standard Cahn–Hilliard equation can be found in various references [25,26].

The parameters for the numerical examples in Section 5 will be given in dimensionless form. Consider therefore a length scale L_0, which is representative of the size of the domain Ω, and time scale $T_0 = L_0^4/D\lambda$. Relevant dimensionless quantities, denoted with an asterisk, are given by:

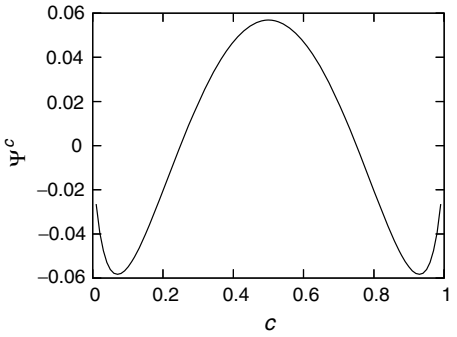

Fig. 1. Non-convex chemical free-energy Ψ^c as a function of concentration.

$$t^\star = t/T_0, \quad x^\star = x/L_0, \quad \mu_c^\star = \mu_c L_0^2/\lambda. \tag{10}$$

Using these, the dimensionless counterpart of Eq. (1) is given by:

$$c_{,t^\star} = \nabla^\star \cdot \beta \nabla^\star (\mu_c^\star - \nabla^{\star 2} c), \tag{11}$$

where β is a dimensionless term reflecting the nature of the mobility. In the case of constant mobility $\beta = 1$, and in case of degenerate mobility $\beta = c(1-c)$.

3. Galerkin finite element formulations

In this section, the proposed discontinuous Galerkin formulation is presented. For the later comparison of numerical results, a conventional mixed formulation is also summarised. To this end, we introduce a partition of Ω into n_{el} open sets, Ω_e, each with boundary $\Gamma_e = \partial\Omega_e$:

$$\Omega = \overline{\bigcup_{e=1}^{n_{\text{el}}} \Omega_e}, \quad \text{such that } \bigcap_{e=1}^{n_{\text{el}}} \Omega_e = \emptyset. \tag{12}$$

We will also use the following terminology in the discontinuous Galerkin formulation:

The union of inter-element boundaries and the boundary Γ_q:

$$\widetilde{\Gamma} = \left(\bigcup_{e=1}^{n_{\text{el}}} \Gamma_e \right) \Big\backslash \Gamma_r, \tag{13}$$

which can also be expressed as

$$\widetilde{\Gamma} = \bigcup_{i=1}^{n_i} \Gamma_i. \tag{14}$$

where Γ_i is an element edge, excluding those which are part of Γ_r, and n_i is the number of edges which are not part of Γ_r.

The union of element interiors:

$$\widetilde{\Omega} = \bigcup_{e=1}^{n_{\text{el}}} \Omega_e. \tag{15}$$

The jump operator on a vector:

$$[\![\boldsymbol{a}]\!] = \boldsymbol{a}_1 \cdot \boldsymbol{n}_1 + \boldsymbol{a}_2 \cdot \boldsymbol{n}_2, \quad \text{on } \widetilde{\Gamma} \setminus \Gamma, \tag{16}$$

$$[\![\boldsymbol{a}]\!] = \boldsymbol{a} \cdot \boldsymbol{n} \quad \text{on } \Gamma, \tag{17}$$

where the subscripts refer to the face of the element on either side of each inter-element boundary, and $\boldsymbol{n}$ is the unit outward normal to an element boundary.

The average operator:

$$\langle a \rangle = \frac{1}{2}(a_1 + a_2) \quad \widetilde{\Gamma} \setminus \Gamma, \tag{18}$$

$$\langle a \rangle = a \quad \text{on } \Gamma. \tag{19}$$

where again the subscripts refer to the face of the element on either side of each inter-element boundary. The jump and average operators operate at boundaries only.

We also make repeated use of the standard notation for L_2-inner products:

$$(u, v)_{\Psi} = \int_{\Psi} uv \, \mathrm{d}\Psi. \tag{20}$$

3.1. Discontinuous Galerkin formulation

Let $c^h \in S^h$ be the finite dimensional approximation of the concentration field, where

$$S^h = \{c^h | c^h \in H^1(\Omega),\ c^h \in P^k(\Omega_e)\ \forall e,\ c^h = g \text{ on } \Gamma_g\}, \tag{21}$$

with $P^k(\Omega_e)$ being the space of the standard polynomial finite element shape functions on element Ω_e where k is the polynomial order. It has been assumed implicitly that g comes from a space such that it can be represented exactly by the finite element basis functions. Let $w^h \in V^h$ be the finite dimensional weighting function, where

$$V^h = \{w^h | w^h \in H^1(\Omega),\ w^h \in P^k(\Omega_e)\ \forall e,\ w^h = 0 \text{ on } \Gamma_g\}. \tag{22}$$

Note that these function spaces possess less regularity than would be required in a conventional formulation for the Cahn–Hilliard equation. A conventional Galerkin formulation would seek solutions in a subspace of $H^2(\Omega)$, rather than in subspaces of $H^1(\Omega)$. An approximate solution to the Cahn–Hilliard equation then involves: find $c^h \in S^h \times [0, T]$ such that

$$\begin{aligned}
&(w^h, \dot{c}^h)_{\Omega} + (\nabla w^h, M^h \nabla \mu_c^h)_{\Omega} + (\nabla^2 w^h, M^h \lambda \nabla^2 c^h)_{\tilde{\Omega}} + (\nabla w^h, (\nabla M^h) \lambda \nabla^2 c^h)_{\tilde{\Omega}} - (\llbracket \nabla w^h \rrbracket, \langle M^h \lambda \nabla^2 c^h \rangle)_{\tilde{\Gamma}} \\
&\quad - \left(\langle M^h \lambda \nabla^2 w^h \rangle, \llbracket \nabla c^h \rrbracket\right)_{\tilde{\Gamma}} + \left(\frac{\alpha}{\langle h_e \rangle} \llbracket \nabla w^h \rrbracket, M^h \lambda \llbracket \nabla c^h \rrbracket\right)_{\tilde{\Gamma}} \\
&= (w^h, s)_{\Gamma_s} + (\nabla w^h \cdot \boldsymbol{n}, r)_{\Gamma_r} + \left(\frac{\alpha}{h_e} \nabla w^h \cdot \boldsymbol{n}, q\right)_{\Gamma_q} - (\nabla^2 w^h, q)_{\Gamma_q} \quad \forall w^h \in V^h,
\end{aligned} \tag{23}$$

$$(w^h, c^h(\boldsymbol{x}, 0))_{\Omega} = (w^h, c_0(\boldsymbol{x}))_{\Omega} \quad \forall w^h \in V^h, \tag{24}$$

where α is a dimensionless parameter and h_e is a measure of the size of element e. Apart from the boundary condition on the concentration (2) that is built into trial and weighting function spaces, all other boundary conditions are weakly imposed. In particular, the boundary condition on the normal derivative of the concentration, $M\lambda\nabla c \cdot \boldsymbol{n}$, has been imposed in a fashion analogous to Nitsche's method [19]. The same concept has been applied to internal element boundaries to ensure weak continuity of $M^h\lambda\nabla c^h \cdot \boldsymbol{n}$, inspired by the interior penalty method for second-order equations [17] and the later work of Engel et al. [22] for fourth-order elliptic equations. The last term on the left hand-side is the so-called interior penalty term, and is essential for stability. Various terms in the weak form ensure consistency with the governing equation and boundary conditions, which is elaborated in Appendix A.1. The need for the stabilising term is elucidated in Appendix A.2 through an existence analysis of the proposed discontinuous Galerkin formulation. Also worth noting is that the presented weak form holds for non-constant M. In particular, the fourth term on the left hand-side of Eq. (23) vanishes for constant mobility, $\nabla M = 0$. An a priori error estimate for the method is developed in Appendix A.3, which shows in a particular norm that the convergence rate is unaffected by α, although increasing α will have a detrimental effect on the magnitude of the error.

3.2. Mixed finite element formulation

To develop a conventional finite element formulation, consider replacing the fourth-order equation in Eq. (1) by two second-order equations,

$$c_{,t} = \nabla \cdot (M\nabla(\mu_c - \kappa)), \tag{25}$$

$$\kappa = \lambda\nabla^2 c. \tag{26}$$

For the mixed formulation it is convenient to redefine the boundary condition on Γ_q (Eq. (3)) such that

$$\lambda\nabla c \cdot \boldsymbol{n} = q \quad \text{on } \Gamma_q \times (0,T). \tag{27}$$

Then, considering the function spaces:

$$S^h = \{c^h | c^h \in H^1(\Omega), c^h \in P^k(\Omega_e) \forall e, c^h = g \text{ on } \Gamma_g\}, \tag{28}$$

$$V^h = \{w^h | w^h \in H^1(\Omega), w^h \in P^k(\Omega_e) \forall e, w^h = 0 \text{ on } \Gamma_g\}, \tag{29}$$

$$P^h = \{\kappa^h | \kappa^h \in H^1(\Omega), \kappa^h \in P^k(\Omega_e) \forall e, \kappa^h = r \text{ on } \Gamma_r\}, \tag{30}$$

$$Q^h = \{v^h | v^h \in H^1(\Omega), v^h \in P^k(\Omega_e) \forall e, v^h = 0 \text{ on } \Gamma_r\}, \tag{31}$$

where it has been assumed that the boundary conditions g and r can be represented exactly by the finite element basis. Following the standard procedure of integration by parts, and insertion of the Neumann boundary conditions, the Galerkin problem reads: find $c^h \in S^h \times [0,T]$ and $\kappa^h \in P^h$ such that

$$(w^h, c^h_{,t})_\Omega + (\nabla w^h, M^h\nabla(\mu^h_c - \kappa^h))_\Omega = (w^h, s)_{\Gamma_s} \quad \forall w^h \in V^h, \tag{32}$$

$$(v^h, \kappa^h)_\Omega + (\nabla v^h, \lambda\nabla c^h)_\Omega = (v^h, q)_{\Gamma_q} \quad \forall v^h \in Q^h, \tag{33}$$

$$(w^h, c(\boldsymbol{x}, 0))_\Omega = (w^h, c_0(\boldsymbol{x}))_\Omega \quad \forall w^h \in V^h. \tag{34}$$

4. Numerical implementation of the discontinuous Galerkin and mixed finite element formulations

The proposed discontinuous Galerkin method entails in addition to the usual integration over element volumes, integration over inter-element boundaries. While this step is not standard in continuous Galerkin finite element codes, the structure of the necessary code is not dissimilar to the usual loop over element volumes. Numerical implementation of the mixed formulation is identical to the usual implementation for mixed finite element problems.

The proposed discontinuous Galerkin formulation involves an element length scale h_e which is related to the element size. In all simulations, h_e is computed for each element based on the element volume. In the examples presented in Section 5, for triangular elements $h_e = \sqrt{2A_e}$, where A_e is the element area, and for quadrilateral elements $h_e = \sqrt{A_e}$, where A_e is again the element area.

All examples are marched in time using the Crank–Nicolson scheme. At this stage, no adaptive time stepping has been used. The use of adaptive time stepping is potentially very attractive since the concentration field typically evolves rapidly at the start of a simulation before slowing, and then speeding up intermittently as 'bubbles' diffuse and vanish. In order to solve the nonlinear equations, the proposed formulation has been linearised consistently and a Newton–Raphson scheme has been used.

5. Numerical examples and comparison of formulations

5.1. Discretisation comparison

The proposed formulation is first examined for a series of simulations on a unit square $\Omega = (-0.5, 0.5) \times (-0.5, 0.5)$ for a range of discretisations and element types, with the proposed discontinuous Galerkin method compared to the standard mixed formulation. Boundary conditions are specified on $\Gamma_q = \Gamma_s = \Gamma$ (see Section 2), with $q = s = 0$ (see Eqs. (4) and (5)). Considering a square subdomain Ω_1 inside the unit square,

$\Omega_1 = [-0.2, 0.2] \times [-0.2, 0.2]$, and its complement Ω_2, $\Omega = \Omega_1 \cup \Omega_2$, the initial conditions for this test are given by

$$c(\boldsymbol{x}, 0) = \begin{cases} 0.71 & \boldsymbol{x} \in \Omega_1, \\ 0.69 & \boldsymbol{x} \in \Omega_2. \end{cases} \tag{35}$$

These initial conditions are illustrated in Fig. 2. Model parameters are: $\omega/kT = 3$, $NkTL_0^2/\lambda = 600$, $\beta = 1$ (constant mobility), $\alpha = 5$ and $\Delta t^* = 2 \times 10^{-7}$.

Three meshes using the the discontinuous Galerkin formulation and one using the mixed formulation are tested and the concentration contours at $t^* = 8 \times 10^{-5}$ are shown in Fig. 3. The structured mesh of six-noded triangular elements (T6) is composed of 11250 elements, the unstructured mesh of six-noded triangular elements is composed of 10283 elements, the structured mesh of nine-noded quadrilateral elements (Q9) is composed of 10000 elements and the mixed formulation uses 6400 four-noded quadrilateral elements (Q4Q4), with both c^h and κ^h using bilinear shape functions. Clearly, the computed result is insensitive to the nature of the spatial discretisation.

5.2. Influence of the penalty parameter α

The same test is now used to study the influence of the penalty parameter α for the discontinuous Galerkin formulation. In a multi-dimensional setting the influence of α cannot be considered in isolation due to the presence of the element-dependent length scale h_e, the definition of which is not unique. Ideally, α should be as low as possible while still maintaining stability, since error analysis indicates that large values of α have a detrimental effect on accuracy (see Appendix A.3 and Brenner and Sung [27]). Experience indicates that $\alpha = 5$ for the tested elements ensures stability. For $\alpha < 5$, the likelihood of the model being unstable becomes high. The appropriate value of α is dependent on the element type.

Fig. 4 shows the concentration contours at $t^* = 8 \times 10^{-5}$ for the structured T6 mesh and various values of α. For moderate values of α, there is no discernible effect on the results. For the case $\alpha = 50$, a slight bias can be observed in the direction of the triangle diagonals (bottom left-hand side to top right-hand side). Such effects may be observed for large values of α on meshes with a strong, anisotropic bias. However, the effects reduce with mesh refinement. The concentration contours are shown in Fig. 5 for the unstructured T6 mesh with $\alpha = 5$ and $\alpha = 50$. In this case, there is no discernible difference.

The presence of the numerical parameter α, and mesh-dependent length scale h_e, is less than desirable. Fortunately, by drawing on developments in discontinuous Galerkin methods for second-order elliptic equations it is likely that a more sophisticated stabilisation technique will avoid this need and lead to an unconditionally stable method (in the linearised case). This aspect, which is an area of ongoing research, does however often come at the cost of extra computational effort.

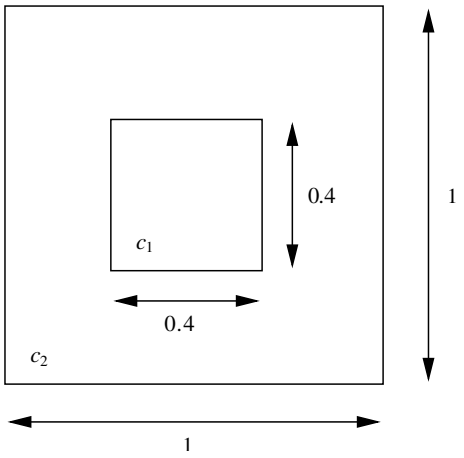

Fig. 2. Initial conditions where $c_1 = 0.71$ and $c_2 = 0.69$.

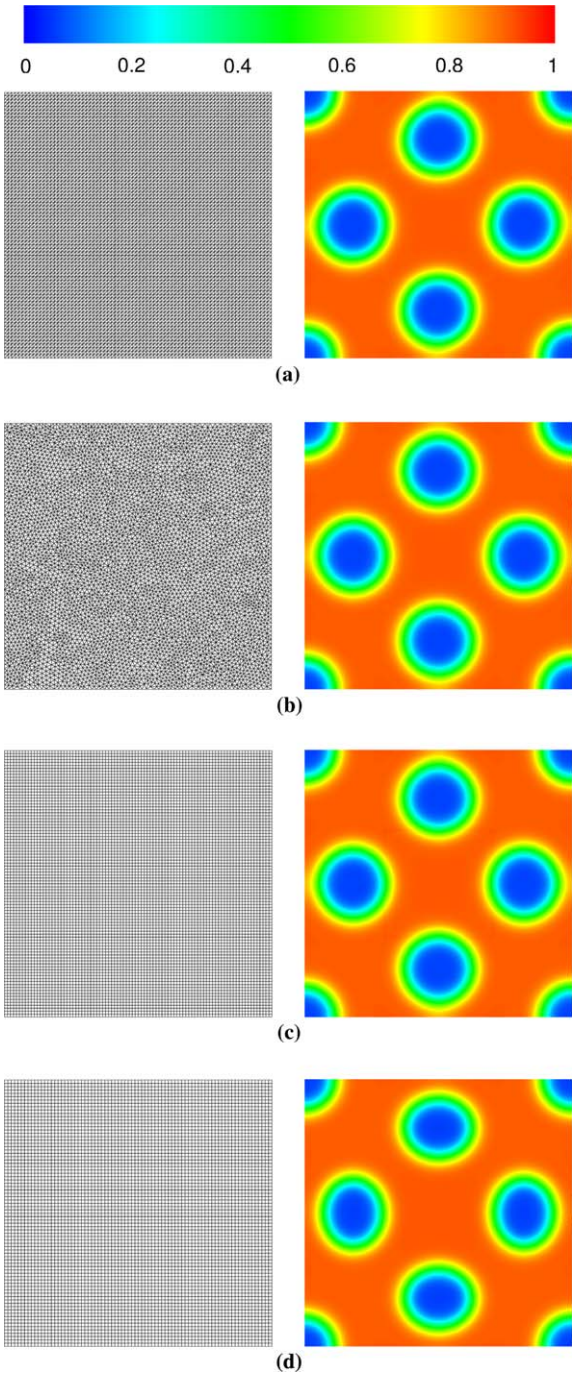

Fig. 3. Finite element meshes (left) and concentration contours (right) for: (a) structured T6 mesh, (b) unstructured T6 mesh, (c) structured Q9 mesh and (d) Q4Q4 mixed method.

5.3. Evolution from a randomly perturbed initial condition

The evolution of the concentration field from a randomly perturbed initial condition is now examined on the unit square domain. For this test, the following parameters have been adopted: $\omega/kT = 3$, $NkTL_0^2/\lambda = 3000$, $\beta = c(1-c)$ (degenerate mobility), $\alpha = 5$ and $\Delta t^* = 2 \times 10^{-8}$. For the initial conditions, the average

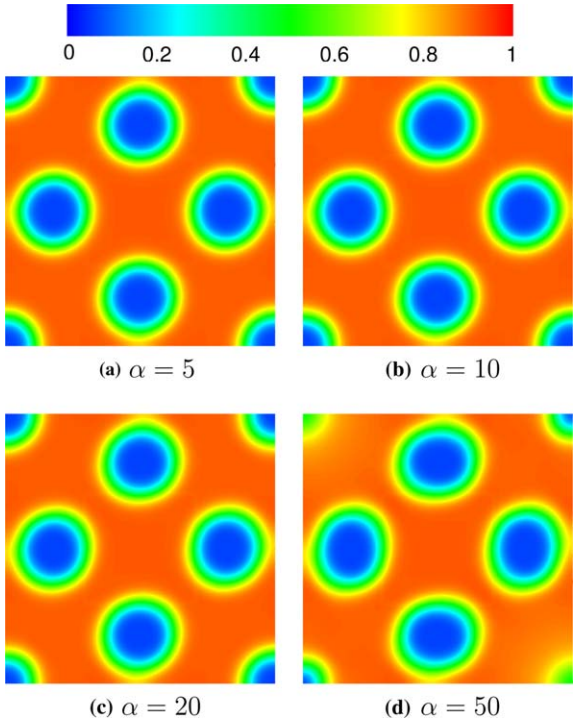

Fig. 4. Influence of the penalty parameter α for the structured T6 mesh.

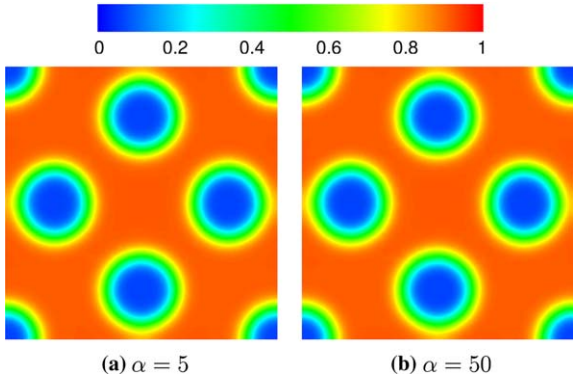

Fig. 5. Influence of the penalty parameter α for the unstructured T6 mesh.

concentration is equal to 0.63, with random fluctuations of zero mean and no fluctuation greater than 0.05. For the sake of comparison, the simulations have been performed for both the discontinuous Galerkin method and the mixed Galerkin formulation. For the discontinuous Galerkin technique, the unstructured T6 mesh shown in Fig. 3(b) has been used, and for the mixed method, the Q4Q4 mesh shown in Fig. 3(d) has been used.

Figs. 6 and 7 show the evolution of the concentration field for the discontinuous and the mixed Galerkin formulations, respectively. Although starting from different initial random perturbations due to the different meshes and basis functions (the initial conditions are identical in the statistical sense), both methods show similarities in capturing the characteristic features of the Cahn–Hilliard equation. The first time snapshots in the

two series differ slightly due to the different initial random perturbations. However, already at $t^\star = 2 \times 10^{-6}$, similar patterns start to develop. The concentration evolution can basically be categorised in two phases: the first phase, which is predominantly governed by spinodal decomposition and phase separation, and a second phase which is characterised by grain coarsening.

During the first phase, roughly corresponding to the first four figures of each series, changes in concentration are driven primarily by the minimisation of the local chemical energy Ψ^c. This period is basically terminated as soon as the local concentration is driven to either value of the two binodal points. The two different discretisation techniques render statistically similar patterns. Approximately from $t^\star = 8 \times 10^{-6}$ onwards, local changes in concentrations are primarily governed by the surface free energy Ψ^s. In order to minimise its contribution, the generated patterns cluster and grains tend to coarsen. This Ostwald ripening takes place on a much longer time scale. Accordingly, grain coarsening is a very slow process and concentrations do not change rapidly between $t^\star = 8 \times 10^{-6}$ and $t^\star = 2.56 \times 10^{-4}$. Again, Figs. 6 and 7 show a statistically similar response as the grain sizes and the number of grains are of the same order of magnitude for each depicted time

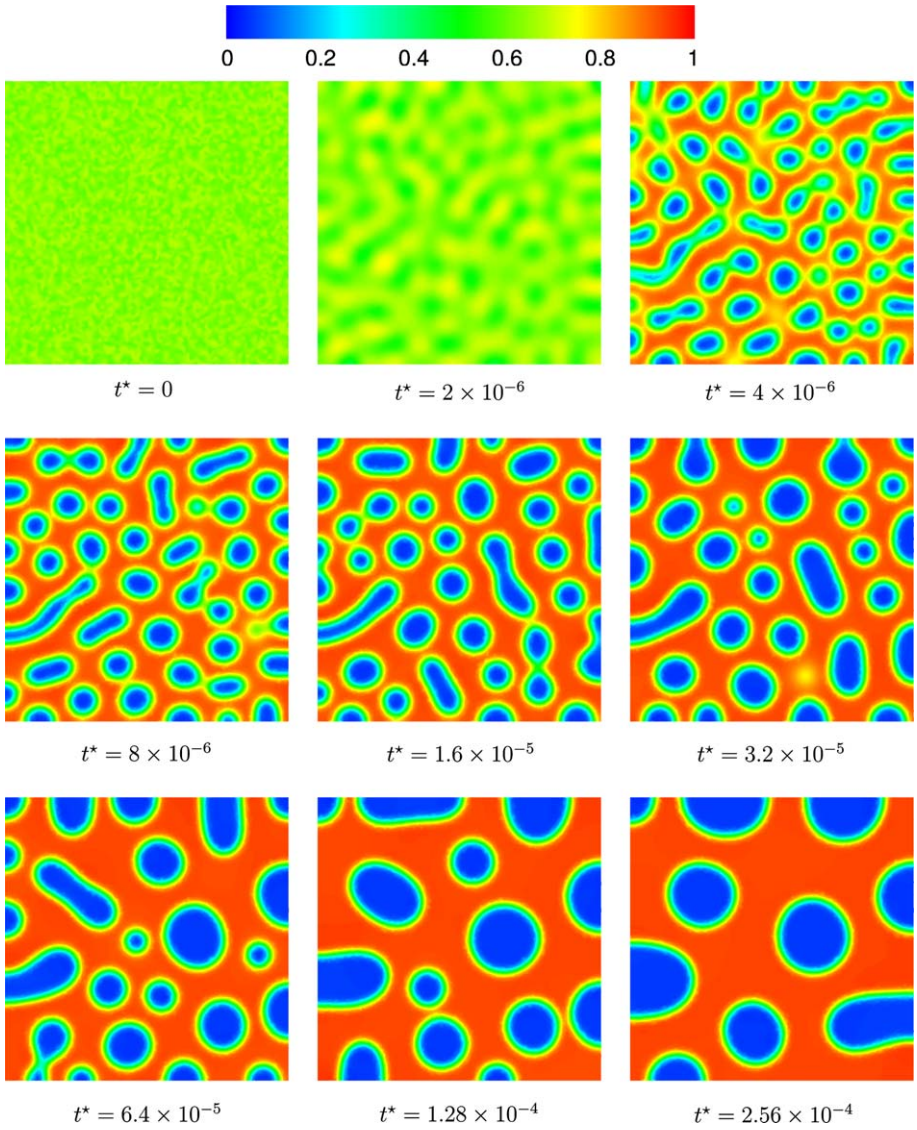

Fig. 6. Evolution of concentration contours from a randomly perturbed initial condition using the discontinuous Galerkin method.

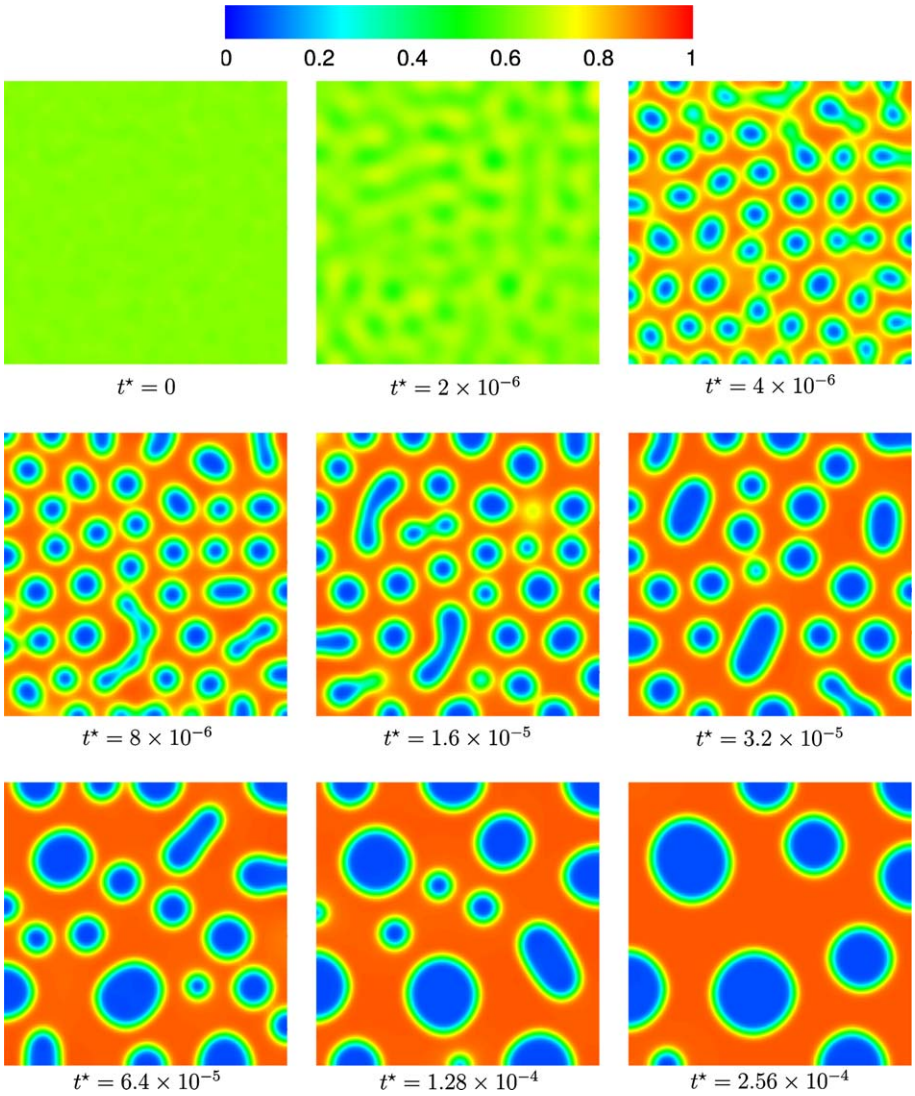

Fig. 7. Evolution of concentration contours from a randomly perturbed initial condition using a mixed finite element method.

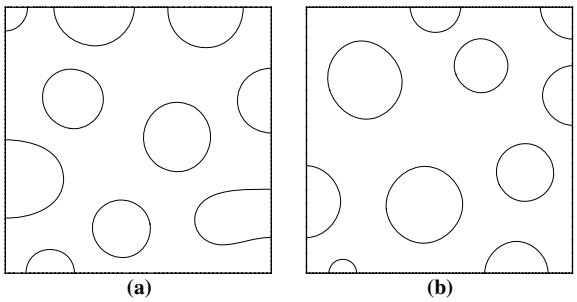

Fig. 8. Contours at $c = 0.5$ and $t^\star = 2.56 \times 10^{-4}$ for the (a) discontinuous Galerkin and (b) mixed formulation.

step. To emphasise this, for the two methods a plot with a single contour at $c = 0.5$ is presented in Fig. 8 at $t^\star = 2.56 \times 10^{-4}$. The total length of the contours for the two formulations is very close: 5.26 for the discontinuous Galerkin formulation and 5.00 for the mixed formulation.

6. Conclusions

The formulation presented in this paper allows for the solution of the Cahn–Hilliard equation in primal form using simple C^0 finite element basis functions. The variational problem has been shown to be consistent with the Cahn–Hilliard equation, stability is assured for a sufficiently large penalty parameter, and an a priori estimate is provided for the error in an energy-type norm.

While not demonstrated for the Cahn–Hilliard equation in this paper, the proposed formulation represents a promising avenue for development of efficient linear solvers methods for the Cahn–Hilliard equation. Recent developments in multigrid methods for this class of problem [28] hold significant promise. This is of particular relevance given the computationally intensive nature of this problem, and effective iterative linear solvers will be invaluable tools for well-resolved three-dimensional simulations.

Acknowledgements

G.N. Wells was supported by the Netherlands Technology Foundation STW, applied science division of NWO and the technology programme of the Ministry of Economic Affairs. K. Garikipati was supported by a Presidential Early Career Award for Scientists and Engineers through the US Department of Energy, and the Alexander von Humboldt Foundation of Germany. He also wishes to express his gratitude to Universität Stuttgart for hosting him while on the Humboldt fellowship.

Appendix A. Analysis of the discontinuous Galerkin formulation

A.1. Consistency: Euler–Lagrange equations

The repeated application of integration by parts on Eq. (23) leads to:

$$\begin{aligned}(w^h, c^h_{,t})_\Omega - (w^h, \nabla\cdot M^h\nabla(\mu^h_c - \lambda\nabla^2 c^h))_{\tilde\Omega} + (w^h, [\![M^h\nabla(\mu^h_c - \lambda\nabla^2 c^h)]\!])_{\tilde\Gamma\setminus\Gamma_q} + (\langle\nabla w^h\rangle, [\![M^h\lambda\nabla^2 c^h]\!])_{\tilde\Gamma\setminus\Gamma_q}\\ + (\frac{\alpha}{\langle h_e\rangle}[\![\nabla w^h]\!] - \langle\nabla^2 w^h\rangle, [\![M^h\lambda\nabla c^h]\!])_{\tilde\Gamma\setminus\Gamma_q} + (w^h, M^h\nabla(\mu^h_c - \lambda\nabla^2 c^h)\cdot\boldsymbol{n} - s)_{\Gamma_s} + (\nabla w^h\cdot\boldsymbol{n}, M^h\lambda\nabla^2 c^h - r)_{\Gamma_r}\\ + (\frac{\alpha}{\langle h_e\rangle}\nabla w^h\cdot\boldsymbol{n} - \nabla^2 w^h, M^h\lambda\nabla c^h\cdot\boldsymbol{n} - q)_{\Gamma_q} = 0,\end{aligned} \tag{A.1}$$

where we have used

$$(\nabla\cdot(M\nabla w), (\lambda\nabla^2 c))_\Omega = (\nabla M\cdot\nabla w, (\lambda\nabla^2 c))_\Omega + (M\nabla^2 w, (\lambda\nabla^2 c))_\Omega. \tag{A.2}$$

These results, together with Eq. (24), imply the weak imposition of the following equations and continuity conditions

$$c^h_{,t} = \nabla\cdot(M^h\nabla(\mu^h_c - \lambda\nabla^2 c^h)) \quad \text{in } \widetilde\Omega\times(0,T), \tag{A.3}$$

$$[\![M^h\nabla c^h]\!] = 0 \quad \text{on } \widetilde\Gamma\setminus\Gamma_q\times(0,T), \tag{A.4}$$

$$[\![M^h\lambda\nabla^2 c^h]\!] = 0 \quad \text{on } \widetilde\Gamma\setminus\Gamma_q\times(0,T), \tag{A.5}$$

$$[\![M^h\nabla(\mu^h_c - \lambda\nabla^2 c^h)]\!] = 0 \quad \text{on } \widetilde\Gamma\setminus\Gamma_q\times(0,T), \tag{A.6}$$

$$M^h\lambda\nabla c^h\cdot\boldsymbol{n} = q \quad \text{on } \Gamma_q\times(0,T), \tag{A.7}$$

$$M^h\lambda\nabla^2 c^h = r \quad \text{on } \Gamma_r\times(0,T), \tag{A.8}$$

$$M^h\nabla(\mu^h_c - \lambda\nabla^2 c^h)\cdot\boldsymbol{n} = s \quad \text{on } \Gamma_s\times(0,T), \tag{A.9}$$

showing that the proposed formulation is consistent with the Cahn–Hilliard equation and associated boundary conditions. This process illustrates the roles played by different non-standard terms in the weak formulation in implying the appropriate Euler–Lagrange equations.

A.2. Existence of a solution: time continuous case

The need for the penalty term in order to stabilise the discontinuous Galerkin formulation is justified in this section. The standard L_2 norm over Ω is denoted $\|c\|$, and when implying integration over another domain, the domain is given, for example,

$$\|\nabla^2 c\|_{\tilde{\Omega}}^2 = \int_{\tilde{\Omega}} (\nabla^2 c)^2 \,\mathrm{d}\Omega. \tag{A.10}$$

To prove existence of a solution to the discontinuous Galerkin model, analysis techniques commonly used to prove existence of weak solutions to the Cahn–Hilliard equation are followed (see, for example, Elliott and Zheng [14]) and extended where necessary for the discontinuous Galerkin case. The goal is to show that the concentration field in the proposed formulation is bounded in time, and in terms of a norm on V,

$$\|c\|_V = \|\nabla c\| + \|\nabla^2 c\|_{\tilde{\Omega}} + \sum_i^{n_i} \frac{1}{\langle h_e \rangle} \|[\![\nabla c]\!]\|_{\Gamma_i}, \tag{A.11}$$

where n_i is the number of element boundaries, which is an energy-like norm. Note that $\|c\|_V = 0$ only for the trivial case of constant c. The use of a logarithmic free-energy complicates the analysis considerably due the lack of continuity on the real line. Furthermore, concentration dependent mobility introduces considerable difficulties which have complicated past mathematical analysis of the Cahn–Hilliard equation. At this point, we restrict ourselves to the case of constant mobility, and for simplicity a continuous free energy, as is often used in analysis. Analysis for the case of logarithmic free energy can be found in Copetti and Elliot [29] and Barrett and Blowey [30], and for the case of concentration-dependent mobility in Elliott and Garcke [31] and Barrett et al. [7].

In examining the existence of a solution, a number of inequalities will prove useful and are presented first. The definition of various constants, denoted C, may vary at each appearance. A subscript 'e' is used to denote element-wise constants. From integration by parts and the application of the Cauchy–Schwarz inequality and Young's inequality, it is clear that for all u, $v \in V^h$ (V^h has been defined in Section 3.1):

$$\begin{aligned}
(\nabla u, \nabla v)_\Omega &= -(u, \nabla^2 v)_{\tilde{\Omega}} + \sum_i^{n_i} (u, [\![\nabla v]\!])_{\Gamma_i} \leqslant |(u, \nabla^2 v)_{\tilde{\Omega}}| + \sum_i^{n_i} |(u, [\![\nabla v]\!])_{\Gamma_i}| \\
&\leqslant \|u\| \|\nabla^2 v\|_{\tilde{\Omega}} + \sum_i^{n_i} (\|u\|_{\Gamma_i} \|[\![\nabla v]\!]\|_{\Gamma_i}) \\
&\leqslant \epsilon_0 \|u\|^2 + \frac{1}{4\epsilon_0} \|\nabla^2 v\|_{\tilde{\Omega}}^2 + \sum_i^{n_i} \langle \epsilon_{1,e} \rangle \|u\|_{\Gamma_i}^2 + \frac{1}{4} \sum_i^{n_i} \frac{1}{\langle \epsilon_{1,e} \rangle} \|[\![\nabla v]\!]\|_{\Gamma_i}^2,
\end{aligned} \tag{A.12}$$

where ϵ_0, $\epsilon_{1,e} > 0$. The term $\epsilon_{1,e}$ may vary for each element. Considering the discrete trace inequality (see [18, Eq. (2.4)]),

$$\|u\|_{\partial\Omega_e}^2 \leqslant \frac{C_e}{h_e} \|u\|_{\Omega_e}^2 + C_e h_e \|\nabla u\|_{\Omega_e}^2 \quad \forall u \in H^1(\Omega_e), \tag{A.13}$$

and the inverse estimate [32, Eq. (4.5.7)]

$$\|\nabla u\|_{\Omega_e}^2 \leqslant \frac{C_e}{h_e^2} \|u\|_{\Omega_e}^2 \quad \forall u \in H^1(\Omega_e), \tag{A.14}$$

it is possible to bound the term $\sum_i^{n_i} \langle \epsilon_{1,e} \rangle \|u\|_{\Gamma_i}^2$ in terms of a norm over element volumes,

$$\sum_i^{n_i} \langle \epsilon_{1,e} \rangle \|u\|_{\Gamma_i}^2 \leqslant \sum_e^{n_e} \epsilon_{1,e} \frac{C_e}{h_e} \|u\|_{\Omega_e}^2, \tag{A.15}$$

where n_e is the number of elements. Using the above result in combination with Eq. (A.12)

$$\|\nabla u\|^2 \leqslant 2\epsilon_0 \|u\|^2 + \frac{1}{4\epsilon_0} \|\nabla^2 u\|_{\tilde{\Omega}}^2 + \frac{1}{4\epsilon_0} \sum_i^{n_i} \frac{1}{\langle h_e / C_e \rangle} \|[\![\nabla u]\!]\|_{\Gamma_i}^2. \tag{A.16}$$

Another useful result involves the term $|(\langle\nabla^2 u\rangle, [\![\nabla v]\!])_{\tilde{\Gamma}}|$. Using the above inequalities, it is possible to show that

$$|(\langle\nabla^2 u\rangle, [\![\nabla v]\!])_{\tilde{\Gamma}}| \leqslant \frac{1}{2}\sum_e^{n_e} \frac{\epsilon_{2,e} C_e}{h_e}\|\nabla^2 u\|^2_{\Omega_e} + \frac{1}{2}\sum_i^{n_i} \frac{1}{\langle\epsilon_{2,e}\rangle}\|[\![\nabla v]\!]\|^2_{\Gamma_i}, \tag{A.17}$$

$\epsilon_{2,e} > 0$. This result compares to Engel et al. [22, Eq. (161)]. These results will be important in demonstrating existence of a solution for the proposed discontinuous Galerkin scheme.

For the boundary conditions $q = s = 0$ with $\Gamma_q = \Gamma_s = \Gamma$ and $M = 1$, setting $w^h = c^h$ in Eq. (23) leads to

$$\frac{1}{2}\frac{\mathrm{d}}{\mathrm{d}t}\|c^h\|^2 + (\nabla c^h, \mu_c'^h \nabla c^h)_\Omega + \lambda\|\nabla^2 c^h\|^2_{\tilde{\Omega}} - 2\lambda([\![\nabla c^h]\!], \langle\nabla^2 c^h\rangle)_{\tilde{\Gamma}} + \alpha\lambda\sum_i^{n_i}\frac{1}{\langle h_e\rangle}\|[\![\nabla c^h]\!]\|^2_{\Gamma_i} = 0, \tag{A.18}$$

where $\mu_c' = \mathrm{d}\mu_c/\mathrm{d}c$. Considering the condition on the chemical free-energy

$$\mu_c' \geqslant -b_0, \quad b_0 > 0, \tag{A.19}$$

which is satisfied by the commonly adopted logarithmic (see Eq. (8)) and quartic free-energy models, leads to the result

$$-(\nabla c^h, \mu_c'^h \nabla c^h)_\Omega \leqslant b_0\|\nabla c^h\|^2 \quad \forall c^h \in V^h. \tag{A.20}$$

Therefore, from Eq. (A.18),

$$\frac{1}{2}\frac{\mathrm{d}}{\mathrm{d}t}\|c^h\|^2 + \frac{1}{2}\|\nabla c^h\|^2 + \lambda\|\nabla^2 c^h\|^2_{\tilde{\Omega}} + \alpha\lambda\sum_i^{n_i}\frac{1}{\langle h_e\rangle}\|[\![\nabla c^h]\!]\|^2_{\Gamma_i} \leqslant b_1\|\nabla c^h\|^2 + 2\lambda|([\![\nabla c^h]\!], \langle\nabla^2 c^h\rangle)_{\tilde{\Gamma}}|, \tag{A.21}$$

where $b_1 = b_0 + 1/2$. The difficulty at this point is presented by the presence of the $2\lambda([\![\nabla c^h]\!], \langle\nabla^2 c^h\rangle)_{\tilde{\Gamma}}$ term, which is particular to the discontinuous Galerkin formulation. This term vanishes when seeking solutions in the standard space which possesses extra regularity and satisfies the Dirichlet boundary conditions $\{c \in H^2(\Omega), \nabla c \cdot \boldsymbol{n} = 0 \text{ on } \Gamma\}$. To proceed here, the non-standard term must be bounded by some norm. Using the results in Eqs. (A.16) and (A.17), Eq. (A.21) becomes

$$\begin{aligned}&\frac{1}{2}\frac{\mathrm{d}}{\mathrm{d}t}\|c^h\|^2 + \frac{1}{2}\|\nabla c^h\|^2_\Omega + \lambda\|\nabla^2 c^h\|^2_{\tilde{\Omega}} + \alpha\lambda\sum_i^{n_i}\frac{1}{\langle h_e\rangle}\|[\![\nabla c^h]\!]\|^2_{\Gamma_i}\\ &\quad\leqslant 2b_1\epsilon_0\|c^h\|^2 + \sum_e^{n_e}\left(\frac{b_1}{4\epsilon_0} + \frac{\lambda\epsilon_{2,e}C_e}{h_e}\right)\|\nabla^2 c^h\|^2_{\Omega_e} + \sum_i^{n_i}\left(\frac{b_1}{4\epsilon_0\langle h_e/C_e\rangle} + \frac{\lambda}{\langle\epsilon_{2,e}\rangle}\right)\|[\![\nabla c^h]\!]\|^2_{\Gamma_i}.\end{aligned} \tag{A.22}$$

Defining now $\epsilon_0 = b_1/4\lambda\epsilon_0'$ and $\epsilon_{2,e} = \epsilon_2' h_e/C_e$, where $\epsilon_0', \epsilon_2' > 0$, and rearranging the terms in the above equation and multiplying both sides by a factor two,

$$\begin{aligned}&\frac{\mathrm{d}}{\mathrm{d}t}\|c^h\|^2 + \|\nabla c^h\|^2_\Omega + 2\lambda(1 - \epsilon_0' - \epsilon_2')\|\nabla^2 c^h\|^2_{\tilde{\Omega}}\\ &\quad + 2\lambda\sum_i^{n_i}\left(\frac{\alpha}{\langle h_e\rangle} - \frac{\epsilon_0'}{\langle h_e/C_e\rangle} - \frac{1}{\epsilon_2'\langle h_e/C_e\rangle}\right)\|[\![\nabla c^h]\!]\|^2_{\Gamma_i} \leqslant \frac{b_1^2}{\lambda\epsilon_0'}\|c^h\|^2.\end{aligned} \tag{A.23}$$

Consider ϵ_0' to be very small (approaching zero) and $\epsilon_2' < 1 - \epsilon_0'$. In the limit as ϵ_0' approaches zero, if $\alpha > C$, where $C = \max(C_e)$ and C_e is defined by Eq. (A.15), then all terms on the LHS are positive. However, the terms on the RHS will be proportional to $1/\epsilon_0'$. For $\epsilon_0' = 1/4$ and $\epsilon_1' = 1/2$, if

$$\alpha > C\left(4 + \frac{1}{4}\right), \tag{A.24}$$

then all terms on the LHS are positive and the necessary bounds can be developed from Gronwall inequalities, as is done in standard analysis of the Cahn–Hilliard equation. For $\epsilon_0' = 1/4$ and $\epsilon_1' = 1/2$, using Gronwall's inequality, for $0 \leqslant t \leqslant T$ it holds that

$$\|c^h(t)\|^2 \leqslant \|c_0^h\|^2 \mathrm{e}^{4b_1^2 T/\lambda}, \tag{A.25}$$

which implies that

$$\|c^h\|^2_{L^\infty(0,T;L^2(\Omega))} = \max_{0\leqslant t\leqslant T}\|c^h(t)\|^2 \leqslant C_T\|c_0^h\|^2, \tag{A.26}$$

where C_T depends only on b_1, T and λ. Hence, the concentration field is bounded for all $t \leqslant T$ in terms of the initial conditions. Integrating Eq. (A.23) with respect to time from $t = 0$ to $t = T$,

$$\int_0^T \|\nabla c^h\|^2 \,\mathrm{d}t \leqslant \frac{4b_1^2}{\lambda} \int_0^T \|c\|^2 \,\mathrm{d}t, \tag{A.27}$$

which when considering Eq. (A.26) implies that

$$\int_0^T \|\nabla c^h\|^2 \,\mathrm{d}t \leqslant C\|c_0^h\|^2. \tag{A.28}$$

Repeating this procedure for each of the $\|\nabla^2 c^h\|_{\tilde{\Omega}}$ and $\|[\![\nabla c^h]\!]\|_{\tilde{\Gamma}}$ terms on the LHS of Eq. (A.23) leads to the result

$$\|c^h\|^2_{L^2(0,T;V(\Omega))} = \int_0^T \|c^h\|_V^2 \,\mathrm{d}t \leqslant C_T\|c_0^h\|^2. \tag{A.29}$$

This is sufficient to prove existence of a solution in the defined space, conditional upon a sufficiently large α satisfying Eq. (A.24).

A.3. Error estimate for the semi-discrete problem

Bounds for the error in an energy-like norm are presented in this section under the assumptions adopted in the previous section in examining stability. Consider the decomposition of the error e such that

$$e = c - c^h = (c - \bar{c}) + (\bar{c} - c^h) = \eta + e^h, \tag{A.30}$$

where $\bar{c} \in V^h$ is the nodal interpolant of the exact solution, η is the interpolation error, $\eta = c - \bar{c}$, and $e^h = \bar{c} - c^h$. Given that c^h is the solution to Eq. (23) and that the proposed formulation is consistent,

$$\begin{aligned}
&(w^h, e^h_{,t})_\Omega + (\nabla^2 w^h, \lambda\nabla^2 e^h)_{\tilde{\Omega}} + \sum_i^{n_i} \frac{\lambda\alpha}{\langle h_e\rangle}([\![\nabla w^h]\!], [\![\nabla e^h]\!])_{\Gamma_i} \\
&\quad \leqslant |(w^h, \eta_{,t})_\Omega| + |(\nabla w^h, \nabla\mu_c(c) - \nabla\mu_c(c^h))_\Omega| + |(\nabla^2 w^h, \lambda\nabla^2\eta)_{\tilde{\Omega}}| + |([\![\nabla w^h]\!], \lambda\langle\nabla^2 e^h\rangle)_{\tilde{\Gamma}}| \\
&\qquad + |(\langle\nabla^2 w^h\rangle, \lambda[\![\nabla e^h]\!])_{\tilde{\Gamma}}| + |([\![\nabla w^h]\!], \lambda\langle\nabla^2\eta\rangle)_{\tilde{\Gamma}}| + |(\langle\nabla^2 w^h\rangle, \lambda[\![\nabla\eta]\!])_{\tilde{\Gamma}}| + \sum_i^{n_i} \frac{\lambda\alpha}{\langle h_e\rangle}|([\![\nabla w^h]\!], [\![\nabla\eta]\!])_{\Gamma_i}|.
\end{aligned} \tag{A.31}$$

Setting $w^h = e^h$ and adding $\|\nabla e^h\|^2$ to both sides of the above equation

$$\begin{aligned}
&\frac{1}{2}\frac{\mathrm{d}}{\mathrm{d}t}\|e^h\|^2 + \|\nabla e^h\|^2 + \lambda\|\nabla^2 e^h\|^2_{\tilde{\Omega}} + \sum_i^{n_i} \frac{\lambda\alpha}{\langle h_e\rangle}\|[\![\nabla e^h]\!]\|^2_{\Gamma_i} \\
&\quad \leqslant |(e^h, \eta_{,t})_\Omega| + \|\nabla e^h\|^2 + |(\nabla e^h, \nabla\mu_c(c) - \nabla\mu_c(c^h))_\Omega| + |(\nabla^2 e^h, \lambda\nabla^2\eta)_{\tilde{\Omega}}| \\
&\qquad + 2|([\![\nabla e^h]\!], \lambda\langle\nabla^2 e^h\rangle)_{\tilde{\Gamma}}| + |([\![\nabla e^h]\!], \lambda\langle\nabla^2\eta\rangle)_{\tilde{\Gamma}}| + |(\langle\nabla^2 e^h\rangle, \lambda[\![\nabla\eta]\!])_{\tilde{\Gamma}}| + \sum_i^{n_i} \frac{\lambda\alpha}{\langle h_e\rangle}|([\![\nabla e^h]\!], [\![\nabla\eta]\!])_{\Gamma_i}|.
\end{aligned} \tag{A.32}$$

A bound is now sought for each term on the RHS of the above equation. It is straightforward to show that

$$|(e^h, \eta_{,t})_\Omega| \leqslant \frac{1}{2}\|e^h\|^2 + \frac{1}{2}\|\eta_{,t}\|^2. \tag{A.33}$$

The second term on the RHS of Eq. (A.32) requires careful attention. Assuming that the gradient of μ_c is Lipschitz continuous,

$$\left\|\nabla\mu_c(c) - \nabla\mu_c\left(c^h\right)\right\| \leqslant C\left\|c - c^h\right\|, \tag{A.34}$$

it holds that

$$|(\nabla e^h, \nabla\mu_c(c) - \nabla\mu_c(c^h))_\Omega| \leqslant \|\nabla e^h\|\|\nabla\mu_c(c) - \nabla\mu_c(c^h)\| \leqslant C\|\nabla e^h\|\|c - c^h\| = C\|\nabla e^h\|\|e^h + \eta\|$$
$$\leqslant C\|\nabla e^h\|(\|e^h\| + \|\eta\|) \leqslant \frac{1}{2}\|\nabla e^h\|^2 + C^2\|e^h\|^2 + C^2\|\eta\|^2. \tag{A.35}$$

From Eq. (A.17), it holds that

$$2|([\![\nabla e^h]\!], \lambda\langle\nabla^2 e^h\rangle)_{\tilde{\Omega}}| \leqslant \frac{\lambda}{2}\|\nabla^2 e^h\|^2_{\Omega_e} + 2\lambda\sum_i^{n_i}\frac{1}{\langle h_e/C_e\rangle}\|[\![\nabla e^h]\!]\|^2_{\Gamma_i} \tag{A.36}$$

and in the same vein,

$$|([\![\nabla e^h]\!], \lambda\langle\nabla^2\eta\rangle)_{\tilde{\Gamma}}| \leqslant 4\lambda\|\nabla^2\eta\|^2_{\tilde{\Omega}} + \frac{\lambda}{16}\sum_i^{n_i}\frac{1}{\langle h_e/C_e\rangle}\|[\![\nabla e^h]\!]\|^2_{\Gamma_i}. \tag{A.37}$$

It can be shown that,

$$|(\langle\nabla^2 e^h\rangle, \lambda[\![\nabla\eta]\!])_{\tilde{\Gamma}}| \leqslant \frac{\lambda}{8}\|\nabla^2 e^h\|^2_{\tilde{\Omega}} + 2\lambda\sum_i^{n_i}\frac{1}{\langle h_e/C_e\rangle}\|[\![\nabla\eta]\!]\|^2_{\Gamma_i} \leqslant \frac{\lambda}{8}\|\nabla^2 e^h\|^2_{\tilde{\Omega}} + C\lambda\sum_e^{n_e}\frac{1}{h_e^2}\|\nabla\eta\|^2_{\Omega_e}, \tag{A.38}$$

where use has been made of

$$\|[\![\nabla u]\!]\|^2_{\Gamma_i} \leqslant 2\|\nabla u_1\cdot\boldsymbol{n}_1\|^2_{\Gamma_i} + 2\|\nabla u_2\cdot\boldsymbol{n}_2\|^2_{\Gamma_i}, \tag{A.39}$$

in which the subscripts denote sides of the element interface (see Section 3), the trace inequality (see [18, Eq. (2.5)])

$$\|\nabla u\cdot\boldsymbol{n}\|^2_{\partial\Omega_e} \leqslant \frac{C_e}{h_e}\|\nabla u\|^2_{\Omega_e} + C_e h_e\|\nabla^2 u\|^2_{\Omega_e} \quad \forall u \in H^2(\Omega_e), \tag{A.40}$$

and the inverse estimate in Eq. (A.14). Considering the term related to the penalty,

$$\lambda\alpha\sum_i^{n_i}\frac{1}{\langle h_e\rangle}|([\![\nabla e^h]\!], [\![\nabla\eta]\!])_{\Gamma_i}| \leqslant \frac{\alpha\lambda}{2}\sum_i^{n_i}\frac{1}{\langle h_e\rangle}\|[\![\nabla e^h]\!]\|^2_{\Gamma_i} + \frac{\alpha\lambda}{2}\sum_i^{n_i}\frac{1}{\langle h_e\rangle}\|[\![\nabla\eta]\!]\|^2_{\Gamma_i}$$
$$\leqslant \frac{\alpha\lambda}{2}\sum_i^{n_i}\frac{1}{\langle h_e\rangle}\|[\![\nabla e^h]\!]\|^2_{\Gamma_i} + C\alpha\lambda\sum_e^{n_e}\frac{1}{h_e^2}\|\nabla\eta\|^2_{\Omega_e}. \tag{A.41}$$

From Eq. (A.16), the term $\|\nabla e^h\|^2$ is bounded by

$$\|\nabla e^h\|^2 \leqslant \frac{8}{\lambda}\|e^h\|^2 + \frac{\lambda}{16}\|\nabla^2 e^h\|^2_{\Omega_e} + \frac{\lambda}{16}\sum_i^{n_i}\frac{1}{\langle h_e/C_e\rangle}\|[\![\nabla e^h]\!]\|^2_{\Gamma_i}. \tag{A.42}$$

It is trivial to show that

$$\left|\left(\nabla^2 e^h, \lambda\nabla^2\eta\right)_{\tilde{\Omega}}\right| \leqslant \frac{\lambda}{16}\|\nabla^2 e^h\|^2_{\tilde{\Omega}} + 4\lambda\|\nabla^2\eta\|^2_{\tilde{\Omega}}. \tag{A.43}$$

Inserting these bounds into Eq. (A.32) and using Eq. (A.14), for α that satisfies the stability condition,

$$\frac{\mathrm{d}}{\mathrm{d}t}\|e^h\|^2 + \|\nabla e^h\|^2 + \lambda\|\nabla^2 e^h\|^2 + C(\alpha)\lambda\sum_i^{n_i}\frac{1}{\langle h_e\rangle}\|[\![\nabla e^h]\!]\|^2_{\Gamma_i}$$
$$\leqslant C\left(\left(1+\frac{1}{\lambda}\right)\|e^h\|^2 + \|\eta_{,t}\|^2 + \|\eta\|^2 + \lambda(1+\alpha)\sum_e^{n_e}\frac{1}{h_e^2}\|\nabla\eta\|^2_{\Omega_e}\right), \tag{A.44}$$

where $C(\alpha)$ increases with increasing α.
Considering the standard interpolation estimates

$$\|\eta\|^2_{\Omega_e} \leqslant Ch_e^{2(k+1)}|c|^2_{H^{k+1}(\Omega_e)}, \tag{A.45}$$
$$\|\nabla\eta\|^2_{\Omega_e} \leqslant Ch_e^{2k}|c|^2_{H^{k+1}(\Omega_e)}, \tag{A.46}$$

and assuming that the error in the initial conditions are such that

$$\|c^h(0) - c(0)\| \leqslant Ch^{k+1}, \tag{A.47}$$

then by integrating Eq. (A.44) with respect to time, applying Gronwall's inequality (knowing that both c and c^h are bounded),

$$\|e^h\|_\Omega^2 + \int_0^T \|\nabla e^h\|_\Omega^2 \,\mathrm{d}t + \int_0^T \lambda \|\nabla^2 e^h\|_\Omega^2 \,\mathrm{d}t + \int_0^T \lambda\alpha \sum_i^{n_i} \frac{1}{\langle h_e \rangle} \|[\![\nabla e]\!]\|_{\Gamma_i}^2 \,\mathrm{d}t \leqslant C_T(c) h^{2(k-1)}, \tag{A.48}$$

where $C_T(c)$ is dependent on c. Also, $C_T(c)$ increases with increasing α. Through application of the triangle inequality,

$$\|e\|_\Omega^2 + \int_0^T \|\nabla e\|_\Omega^2 \,\mathrm{d}t + \int_0^T \lambda \|\nabla^2 e\|_\Omega^2 \,\mathrm{d}t + \int_0^T \lambda\alpha \sum_i^{n_i} \frac{1}{\langle h_e \rangle} \|[\![\nabla e]\!]\|_{\Gamma_i}^2 \,\mathrm{d}t \leqslant C_T(c) h^{2(k-1)}. \tag{A.49}$$

When considering the norm

$$\|e\|_\Omega^2 + \int_0^T \|\nabla e\|_\Omega^2 \,\mathrm{d}t + \int_0^T \|\nabla^2 e\|_\Omega^2 \,\mathrm{d}t + \int_0^T \sum_i^{n_i} \frac{1}{\langle h_e \rangle} \|[\![\nabla e]\!]\|_{\Gamma_i}^2 \,\mathrm{d}t \leqslant C_T(c) h^{2(k-1)}, \tag{A.50}$$

given that $C_T(c)$ increases with increasing α it is clear that a large α has a detrimental effect on the accuracy. It does not however affect the rate of convergence.

References

[1] J.W. Cahn, J.E. Hilliard, Free energy of a nonuniform system-I: Interfacial free energy, The Journal of Chemical Physics 28 (2) (1958) 258–267.

[2] J.W. Cahn, J.E. Hilliard, Free energy of a nonuniform system-III: Nucleation in a 2-component incompressible fluid, The Journal of Chemical Physics 31 (3) (1959) 688–699.

[3] F. Falk, Cahn–Hilliard theory and irreversible thermodynamics, Journal Non-equilibrium Thermodynamics 17 (1) (1992) 53–65.

[4] I.C. Dolcetta, S.F. Vita, R. March, Area-preserving curve-shortening flows: From phase separation to image processing, Interfaces and Free Boundaries 4 (4) (2002) 325–343.

[5] S. Tremaine, On the origin of irregular structure in Saturn's rings, Astronomical Journal 125 (2) (2003) 894–901.

[6] H.-C. Yu, W. Lu, Dynamics of the self-assembly of nanovoids and nanobubbles in solids, Acta Materialia 53 (6) (2005) 1799–1807.

[7] J.W. Barrett, J.F. Blowey, H. Garcke, Finite element approximation of the Cahn–Hilliard equation with degenerate mobility, SIAM Journal of Numerical Analysis 37 (1) (1999) 286–318.

[8] X. Feng, A. Prohl, Analysis of a fully-discrete finite element method for the phase field model and approximation of its sharp interface limits, SIAM Journal of Numerical Analysis 73 (246) (2003) 541–567.

[9] C.M. Elliott, D.A. French, F.A. Milner, A 2nd-order splitting method for the Cahn–Hilliard equation, Numerische Mathematiek 54 (5) (1989) 575–590.

[10] Q. Du, R.A. Nicolaides, Numerical analysis of a continuum model of phase transition, SIAM Journal of Numerical Analysis 28 (5) (1991) 1310–1322.

[11] J.F. Blowey, C.M. Elliott, The Cahn–Hilliard gradient theory for phase separation with non-smooth free energy. Part II: Numerical analysis, European Journal of Applied Mathematics 3 (1992) 147–179.

[12] E. Bansch, P. Morin, R.H. Nochetto, A finite element method for surface diffusion: The parametric case, Journal of Computational Physics 203 (1) (2005) 321–343.

[13] R.L.J.M. Ubachs, P.J.G. Schreurs, M.G.D. Geers, A nonlocal diffuse interface model for microstructure evolution of tin-lead solder, Journal of the Mechanics and Physics of Solids 52 (8) (2004) 1763–1792.

[14] C.M. Elliott, S. Zheng, On the Cahn–Hilliard Equation, Archive for Rational Mechanics and Analysis 96 (4) (1986) 339–357.

[15] C.M. Elliott, D.A. French, A non-conforming finite element method for the two-dimensional Cahn–Hilliard equation, SIAM Journal of Numerical Analysis 26 (4) (1989) 884–903.

[16] F. Brezzi, M. Fortin, Mixed and Hybrid Finite Element Methods, Springer-Verlag, New York, 1991.

[17] J. Douglas, T. Dupont, Interior penalty procedures for elliptic and parabolic Galerkin methods, in: Computing Methods in Applied ScienceLecture Notes in Physics, vol. 58, Springer-Verlag, Heidelberg, 1976.

[18] D.A. Arnold, An interior penalty finite element method with discontinuous elements, SIAM Journal of Numerical Analysis 19 (4) (1982) 742–760.

[19] J.A. Nitsche, Über ein Varitionsprinzip zur Lösung Dirichlet-Problemen bei Verwendung von Teilräumen, die keinen Randbedingungen unteworfen sind, Abh. Math. Sem. Univ. Hamburg 36 (1971) 9–15.

[20] M.F. Wheeler, Elliptic collocation-finite element method with interior penalties, SIAM Journal of Numerical Analysis 15 (1) (1978) 152–161.

[21] D.N. Arnold, F. Brezzi, B. Cockburn, D. Marini, Unified analysis of discontinuous Galerkin methods for elliptic problems, SIAM Journal of Numerical Analysis 39 (5) (2002) 1749–1779.
[22] G. Engel, K. Garikipati, T.J.R. Hughes, M.G. Larson, L. Mazzei, R.L. Taylor, Continuous/discontinuous finite element approximations of fourth-order elliptic problems in structural and continuum mechanics with applications to thin beams and plates, and strain gradient elasticity, Computer Methods in Applied Mechanics and Engineering 191 (34) (2002) 3669–3750.
[23] G.N. Wells, K. Garikipati, L. Molari, A discontinuous Galerkin formulation for a strain gradient-dependent continuum model, Computer Methods in Applied Mechanics and Engineering 193 (33–35) (2004) 3633–3645.
[24] L. Molari, G.N. Wells, K. Garikipati, F. Ubertini, A discontinuous Galerkin method for strain gradient-dependent damage: Study of interpolations and convergence, Computer Methods in Applied Mechanics and Engineering 195 (13–16) (2006) 1480–1498.
[25] J.W. Cahn, On spinodal decomposition, Acta Metallurgica 9 (1961) 795–801.
[26] M.E. Gurtin, Generlized Ginzburg–Landau and Cahn–Hilliard equations based on a microforce balance, Physica D 92 (1996) 178–192.
[27] S.C. Brenner, L.Y. Sung, C^0 interior penalty methods for fourth order elliptic boundary value problems on polygonal domains, Journal of Scientific Computing 22–23 (1–3) (2005) 83–118.
[28] S.C. Brenner, L.Y. Sung, Multigrid algorithms for C^0 interior penalty methods, SIAM Journal of Numerical Analysis 44 (1) (2006) 199–223.
[29] M.I.M. Copetti, C.M. Elliot, Numerical analysis of the Cahn–Hilliard equation with a logarithmic free energy, Numerische Mathematiek 63 (1) (1992) 39–65.
[30] J.W. Barrett, J.F. Blowey, An error bound for the finite element approximation of the Cahn–Hilliard equation with logarithmic free energy, Numerische Mathematiek 72 (1) (1995) 1–20.
[31] C.M. Elliott, H. Garcke, On the Cahn–Hilliard equation with degenerate mobility, SIAM Journal on Mathematical Analysis 27 (2) (1996) 404–423.
[32] S.C. Brenner, L.R. Scott, The Mathematical Theory of Finite Element Methods, Springer, New York, 1994.